

RESPONSE OF YEAST MUTANTS TO EXTRACELLULAR CALCIUM VARIATIONS

PAMELA A. MARSHALL, EDEN E. TANZOSH, FRANCISCO J. SOLIS
AND HAIYAN WANG

Division of Mathematical and Natural Sciences
Arizona State University
Phoenix, AZ 85069-7100, USA

ABSTRACT. We study, both experimentally and through mathematical modeling, the response of wild type and mutant yeast strains to systematic variations of extracellular calcium abundance. We extend a previously developed mathematical model (Cui and Kaandorp, *Cell Calcium*, 39, 337 (2006))[3], that explicitly considers the population and activity of proteins with key roles in calcium homeostasis. Modifications of the model can directly address the responses of mutants lacking these proteins. We present experimental results for the response of yeast cells to sharp, step-like variations in external Ca^{++} concentrations. We analyze the properties of the model and use it to simulate the experimental conditions investigated. The model and experiments diverge more markedly in the case of mutants lacking the Pmc1 protein. We discuss possible extensions of the model to address these findings.

1. Introduction. Studying the response to calcium stress is an important area of research as it naturally appears in many biologically relevant contexts, including fertilization of eggs and muscle contraction. Calcium is necessary for a wide variety of enzymatic functions and is used as a cellular messenger. However, too much calcium in the cell can lead to hyperosmolarity, which changes the cellular ion concentrations and pH and is detrimental to most cellular functions. Thus cells must carefully control their cellular calcium, although extracellular calcium may vary widely.

In many contexts, it is more effective to use a model cellular system than the actual tissue. For example, the budding *Saccharomyces cerevisiae* has been used for over forty years as a model organism for a wide variety of cellular processes. *S. cerevisiae* is a true eukaryote, and as such, has all the cellular organelles that humans do. *S. cerevisiae* also responds to extracellular signals with changes in intracellular chemistry and gene expression. Furthermore, in this yeast, researchers have been able to develop many genetic methods for easy analysis, such as the ability to quickly delete, add, or move genes of interest [5].

Yeast also will respond to extracellular stressors in the way human tissues do, acting to return the intracellular milieu to homeostasis. Homeostasis is the process by which cells respond to intracellular and extracellular changes in rapid and

2000 *Mathematics Subject Classification.* 92C50, 34C60, 92D25.

Key words and phrases. calcium homeostasis, yeast cells, extracellular signaling, ion storage.

dynamic ways to maintain a stable internal environment, conducive to life. Homeostatic responses can include sequestering molecules, pumping ions into the cytosol, moving ions or small molecules into or out of the cell, or gene expression. Thus, these studies greatly benefit of the use of yeast as a model organism, as it shares the basic homeostatic mechanism with more complex organisms and it is much more easily manipulated in the lab.

The complex behavior of the response to calcium stresses has not been fully explored. The intracellular response to extracellular calcium stress is not quantitatively understood, although mathematical modeling will help describe this phenomenon. Furthermore, there have been quantitative descriptions of cellular response to more complex signals, such as increasing extracellular calcium in a step-wise fashion or the cellular response to extracellular calcium and sodium. In this article, we revisit the original model of Cui and Kaandorp [3] that sought to mathematically model the response to an extracellular calcium pulse in *S. cerevisiae*. This model addresses both short and longer time scale phenomenon. Movement and sequestration of molecules occurs on short time scales, such as milliseconds to seconds, while gene expression takes much longer to occur, in the range of fifteen minutes or more.

We address a number of mathematical properties of the model and use it to discuss the properties of four yeast strains. In this model, the activity of key proteins involved in calcium homeostasis are explicitly considered so that their absence in specific mutants is easily implemented in the model. We prove that the model is well behaved with respect to the crucial variables describing the production of new proteins mediated by Crz1p and calcineurin. We also describe the nature of the equilibrium states of the systems after the change in external calcium concentration. The model is used to simulate the response to steep calcium concentration changes of four yeast cell varieties, the wild type and three single mutants. We address the ability of the model to qualitatively reproduce results observed in pulse experiments carried out in our labs. We conclude by proposing modifications to the model that may better reflect the activity of the protein network that regulates calcium.

2. Model. We restate the model proposed by Cui and Kaandorp [3] with some minor changes of notation. The model is based on the control diagram presented in Fig. 1. This model assumes that calcium in the cytosol, at concentration x (in μM), is acquired from the external environment, where it is present at concentration C_{ex} . The calcium ions are brought into the cytosol mainly through an as yet unknown Channel X [4]; however, some have speculated that this uptake may be performed by the known plasma membrane channel, Cch1p/Mid1p [16]. However, whether or not Cch1p/Mid1p is involved is controversial and we will use the nomenclature of [3]. Calcium uptake occurs continuously, and to avoid deviations from the preferred cytosol concentration levels, the calcium ions are pumped into the nucleus, vacuole, endoplasmic reticulum and Golgi apparatus. The model also considers a small depletion of calcium in individual cells due to the growth and division of the cell. The pumping activity of calcium into the vacuole is carried out by the Pmc1 and Vcx1 proteins, while pumping into the endoplasmic reticulum is carried out by Pmr1p [17]. The uptake of calcium and the pumping into the ER and vacuole is assumed to follow Michaelis-Menten dynamics and is on the order of millisecond time scales. The population and activity of these proteins is in turn regulated by the calcium concentration itself. Calcium binds to calmodulin, which in turn activates the protein phosphatase calcineurin. The activation of calmodulin, which in turn

regulates calcineurin, is proposed to follow from a simple calcium binding process. After several minutes, calcineurin indirectly inactivates the Vcx1p vacuolar calcium transport protein [2]. Calcineurin, then in turn, also dephosphorylates Crz1p, which then translocates to the nucleus to stimulate transcription [8, 15]. In the model, h is the total nuclear fraction of Crz1p. This variable is thus the fraction of Crz1p available for transcriptional activity in response to calcium. The nuclear Crz1p stimulates the production of many proteins including Pmc1p, a vacuolar calcium transporter, and Pmr1p, the Golgi calcium transporter. It is assumed that the starting population of activated Crz1p is equal in both cytosol and nucleus. The fraction of the total population of Crz1p present in the nucleus, the nuclear fraction (h), is determined by means of a simple model of transport across the nuclear boundary. The overall activation of Crz1p is assumed to depend on the number of occupied calcium binding sites on calmodulin.

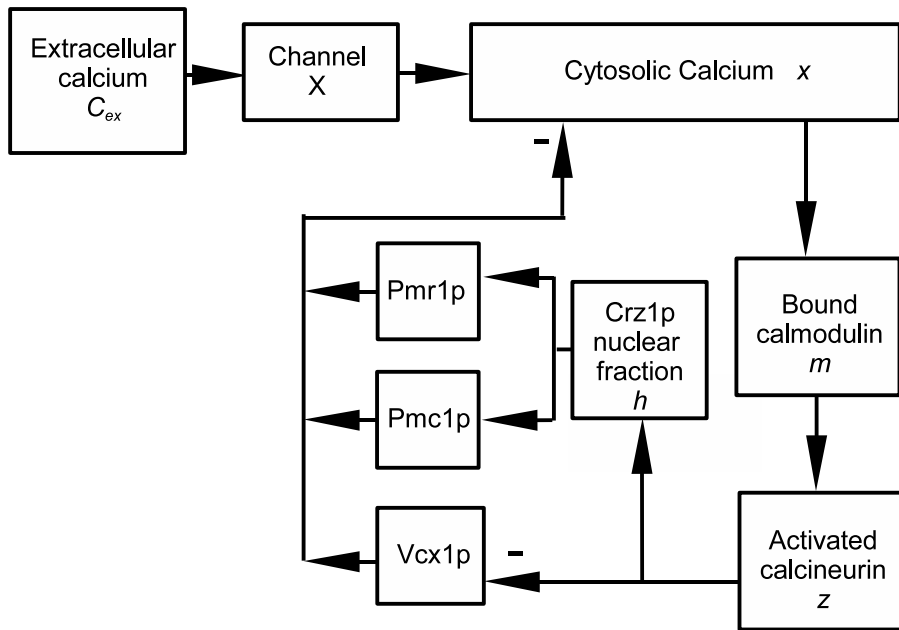


FIGURE 1. Control block diagram of calcium homeostasis, adapted from [3]. We let $m(t)$, $z(t)$, $h(t)$, $x(t)$ denote the concentration of Ca^{2+} -bound calmodulin, the concentration of activated calcineurin, total nuclear fraction of Crz1p, and cytosolic calcium ion concentration respectively. Fig. 1 is the control block diagram of calcium homeostasis. The production of Pmr1p and Pmc1p is proportional to the level of nuclear activation θ , which is gene expression, on a time scale of minutes. The transport of Crz1p into the nucleus occurs in proportion of the transporters activation rate ϕ , on a time scale of seconds. The model discussed above leads to the following set of equations [3]:

We let $m(t), z(t), h(t), x(t)$ denote the concentration of Ca^{2+} -bound calmodulin, the concentration of activated calcineurin, total nuclear fraction, and cytosolic calcium ion concentration respectively. Fig. 1 is the control block diagram of calcium homeostasis. The model discussed above leads to the following set of equations [3]:

$$m' = k_1(c_1 - m)x^3 - k_2m \quad (1)$$

$$z' = k_3(c_2 - z)m - k_4z \quad (2)$$

$$h' = d_1(\phi(z))(1 - h) - d_2(1 - \phi(z))h \quad (3)$$

$$x' = \frac{V_4 C_{ex}}{K_4 + C_{ex}} - [h\theta(z)] \frac{V_1 x}{K_1 + x} - [h\theta(z)] \frac{V_2 x}{K_2 + x} - \frac{1}{1 + k_c z} \frac{V_3 x}{K_3 + x} - \alpha x \quad (4)$$

with initial conditions $m(0) = m_0 \geq 0, z(0) = z_0 \geq 0, h(0) = h_0 \geq 0, x(0) = x_0 \geq 0$, and with $C_{ex} > 0$ a prescribed function of time. These expressions use the functions

$$\phi(z) = \left[1 + \frac{L_0 \left(\left(\frac{\lambda}{z} \right)^{N+1} - 1 \right) \frac{\frac{1}{z} - 1}{\left(\frac{1}{z} \right)^{N+1} - 1}}{\frac{\lambda}{z} - 1} \right]^{-1} \quad (5)$$

and

$$\theta(z) = (1 + L_0) \left[\frac{\left(\frac{1}{z} \right)^{N+1} - 1}{\frac{1}{z} - 1} + \frac{L_0 \left(\left(\frac{\lambda}{z} \right)^{N+1} - 1 \right)}{\frac{\lambda}{z} - 1} \right]^{-1}, \quad (6)$$

where $L_0 = 10^{-N/2}$. The parameters of the model (1-4) were estimated in [3] and references therein. Table A in Appendix A lists values of these parameters and their descriptions.

3. Mathematical analysis. This section addresses three separate mathematical properties of the model. First, we note that the model considers the activity of two of the proteins, Pmr1p and Pmc1p, as modulated by the presence of Crz1p in the nucleus. This modulation appears in the model as a multiplicative factor to the Michaelis-Menten term associated with these proteins. It is then useful to state, in the form of a theorem that these functions have a suitable behavior with respect to their independent variables.

As the variables of the models are the concentrations of specific molecules in the yeast cells, it is important to establish that they satisfy the physical conditions of positivity and boundedness throughout the evolution of the system. The second subsection of the analysis shows that this is the case in this model.

Next, we consider the stability properties of the dynamical system described by the variables x, m, y, z . While an exhaustive analysis of the properties of these points is not possible in general, we state fairly general conditions for their stability and obtain useful formulas that simplify this analysis for specific cases where numerical values of the parameters are specified. The information encoded in the stability properties of the system is relevant to our investigations in two ways. First, it allows to identify the possibility of non-trivial behavior such as stable cycles, or the presence of decaying oscillations in the approach to equilibrium. Both possibilities could be directly observed with common experimental techniques and would validate the assumptions of the model. In addition, explicit characterization of the equilibrium states of the system help the process of numerical analysis by distinguishing between transient but long lived states and the actual final equilibrium condition.

3.1. Properties of ϕ and θ . We shall state ϕ and θ are continuously differentiable functions in this subsection and Lemmas 3.1, 3.2. Their proofs appear in the appendix. The graphs of $\phi(x)$ and $\theta(x)$ are shown in Fig. 2.

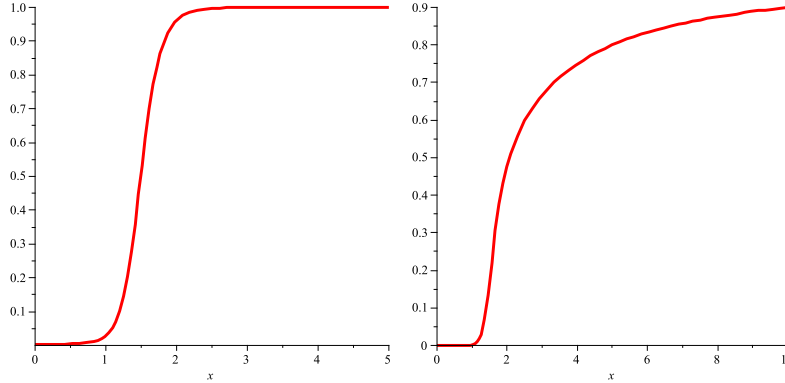


FIGURE 2. Left: graph of $\phi(x)(\lambda = 5, N = 13)$. Right: graph of $\theta(x)(\lambda = 5, N = 13)$

Lemma 3.1. For a positive integer $N > 1$ and $\lambda > 1$, $\phi(x)$ in (5) is defined on $[0, \infty)$. Moreover ϕ is continuously differentiable on $[0, \infty)$, $0 < \phi(x) < 1, \phi'(x) > 0, x \in (0, \infty)$, $0 < \lim_{x \rightarrow 0} \phi(x) < 1$ and $0 < \lim_{x \rightarrow \infty} \phi(x) < 1$. Furthermore, $\lim_{x \rightarrow 0} \phi'(x) = 0$ and $\lim_{x \rightarrow \infty} \phi'(x) = 0$. For $\lambda = 1$, $\phi(x)$ is a positive constant.

Lemma 3.2. For a positive integer $N > 1$ and $\lambda > 1$, $\theta(x)$ in (6) is defined on $[0, \infty)$. Moreover θ is continuously differentiable on $[0, \infty)$, $0 < \theta(x) < 1, \theta'(x) > 0, x \in [0, \infty)$. $\lim_{x \rightarrow 0} \theta(x) = 0, \lim_{x \rightarrow \infty} \theta(x) = 1$. $\lim_{x \rightarrow 0} \theta'(x) = 0, \lim_{x \rightarrow \infty} \theta'(x) = 0$.

3.2. Positiveness and bounded of solutions. We shall show that all solutions exist for all $t > 0$ and bounded from above and below in this subsection.

Lemma 3.3. All solutions of (1-4) exist for $t > 0$, and they are positive and bounded from above.

Proof. Let $(m(t), z(t), h(t), x(t))$ be a solution of the model equations (1-4). Assume $x(t) = 0$ for some $t > 0$. Let $t_0 = \inf\{t : x(t) \leq 0\}$. Then $x(t_0) = 0$ and $x'(t_0) \leq 0$. However,

$$x'(t_0) = \frac{V_4 C_{ex}}{K_4 + C_{ex}} > 0,$$

which is a contradiction. Therefore, $x(t) > 0$ for $t > 0$. By the same argument, $m(t), z(t), h(t)$ are all positive for all $t > 0$.

Now we show the boundedness of the solutions. We start with $h(t)$. Since $0 < \phi(x) < 1, x \in [0, \infty)$, we have

$$h'(t) \leq d_1 - d^* h,$$

where $d^* > 0$ is the lower bound of $d_1 \phi + d_2(1 - \phi)$ on $[0, \infty]$. Therefore,

$$h(t) \leq h(0)e^{-d^* t} + \frac{d_1}{d^*}, \text{ for } t > 0$$

The boundedness also implies that $h(t)$ exists for all $t > 0$. From (4), one can see that

$$x'(t) \leq \frac{V_4 C_{ex}}{K_4 + C_{ex}} - \alpha x,$$

and further

$$\limsup_{t \rightarrow \infty} x(t) \leq \frac{V_4 C_{ex}}{(K_4 + C_{ex})\alpha}. \quad (7)$$

Now from (1), for any $\epsilon > 0$ and some $t_0 > 0$, one has that $x(t) \leq \frac{V_4 C_{ex}}{(K_4 + C_{ex})\alpha} + \epsilon$, for $t > t_0 > 0$,

$$m'(t) \leq k_1 c_1 \left(\frac{V_4 C_{ex}}{(K_4 + C_{ex})\alpha} + \epsilon \right)^3 - k_2 m, \quad t > t_0$$

and

$$m(t) \leq m(t_0) e^{-k_2 t} + \frac{k_1 c_1 \left(\frac{V_4 C_{ex}}{(K_4 + C_{ex})\alpha} + \epsilon \right)^3}{k_2}, \quad t > t_0,$$

which further implies that

$$\limsup_{t \rightarrow \infty} m(t) \leq \frac{k_1 c_1 \left(\frac{V_4 C_{ex}}{(K_4 + C_{ex})\alpha} + \epsilon \right)^3}{k_2}.$$

Thus, letting $\epsilon \rightarrow 0$ gives

$$\limsup_{t \rightarrow \infty} m(t) \leq \frac{k_1 c_1 \left(\frac{V_4 C_{ex}}{(K_4 + C_{ex})\alpha} \right)^3}{k_2}. \quad (8)$$

By the same method, we can get the estimate for $z(t)$

$$\limsup_{t \rightarrow \infty} z(t) \leq \frac{k_3 c_2}{k_4} \frac{k_1 c_1}{k_2} \left(\frac{V_4 C_{ex}}{(K_4 + C_{ex})\alpha} \right)^3. \quad (9)$$

The boundedness of x, h, m, z also implies that they exist for all $t > 0$. \square

We introduce the following notation for upper and lower limits of a function $v(t)$:

$$\bar{v} = \limsup_{t \rightarrow \infty} v(t), \quad \underline{v} = \liminf_{t \rightarrow \infty} v(t).$$

Now, let $(m(t), z(t), h(t), x(t))$ be a solution of (1-4). Lemma 3.3 implies that $\bar{m}, \underline{m}, \bar{z}, \underline{z}, \bar{h}, \underline{h}, \bar{x}, \underline{x}$ are all finite. The well known fluctuation lemma is stated below without proof. Its proof can be found in, e.g., Hirsch et al.[6].

Lemma 3.4. *Let $f : R \rightarrow R$ be a differentiable function. If $l = \liminf_{t \rightarrow \infty} f(t) < \limsup_{t \rightarrow \infty} f(t) = L$, then there are sequences $\{t_k\} \uparrow \infty$, $\{s_k\} \uparrow \infty$ such that for all k , $f'(t_k) = f'(s_k) = 0$, $\lim_{k \rightarrow \infty} f(t_k) = l$ and $\lim_{k \rightarrow \infty} f(s_k) = L$.*

Lemma 3.5. *(1-4) is uniformly persistent, i.e. solutions of (1-4) are eventually uniformly bounded from above and away from zero.*

Proof. We only show that $\underline{x} > 0$. The same argument can be used to show that $\underline{m}, \underline{z}, \underline{h} > 0$. First, if $\underline{x} < \bar{x}$, by the fluctuation lemma, there exist a sequence $\{t'_k\} \uparrow \infty$ such that

$$x'(t'_k) = 0, \quad \lim_{k \rightarrow \infty} x(t'_k) = \underline{x}.$$

Now if we assume $\underline{x} = 0$, (4) gives , for all k ,

$$0 = x'(t'_k) = \frac{V_4 C_{ex}}{K_4 + C_{ex}} - h(t'_k)\theta(z(t'_k))\frac{V_1 x(t'_k)}{K_1 + x(t'_k)} - h(t'_k)\theta(z(t'_k))\frac{V_2 x(t'_k)}{K_2 + x(t'_k)} - \frac{1}{1 + k_c z(t'_k)}\frac{V_3 x(t'_k)}{K_3 + x(t)} - \alpha x(t'_k).$$

Since $\theta(z), h$ are bounded, by taking the limit, we have

$$0 = \frac{V_4 C_{ex}}{K_4 + C_{ex}},$$

which is a contradiction. If $\underline{x} = \bar{x} = 0$, then $\lim_{t \rightarrow \infty} x(t) = 0$. It follows that $\liminf_{t \rightarrow \infty} x'(t) \geq 0$. Thus the boundedness of $x(t)$ implies that $\liminf_{t \rightarrow \infty} x'(t) = 0$. Again, by taking the limit at (4), we have the same contradiction. Thus $\underline{x} > 0$. This completes the proof of the lemma. \square

3.3. Equilibrium and stability. In this section, we establish the existence and uniqueness of the equilibrium of (1-4). Also we shall show that the equilibrium is locally stable by Routh-Hurwitz method.

Theorem 3.6. *There exists a number $\sigma > 0$ such that if $\frac{V_4 C_{ex}}{K_4 + C_{ex}} > \sigma$, the system (1-4) has a unique equilibrium (m^*, z^*, h^*, x^*) .*

Proof. If (m^*, z^*, h^*, x^*) is an equilibrium of (1-4), then

$$m^* = g_1(x^*) := \frac{k_1 c_1 (x^*)^3}{k_1 (x^*)^3 + k_2},$$

$$z^* = g_2(m^*) := \frac{k_3 c_2 m^*}{k_3 m^* + k_4},$$

$$h^* = g_3(z^*) := \frac{d_1 \phi(z^*)}{d_1 \phi(z^*) + d_2 (1 - \phi(z^*))} = \frac{1}{1 + \frac{d_2}{d_1} (\frac{1}{\phi(z^*)} - 1)}.$$

Since g_1, g_2, g_3 are all increasing functions, the composition $h^* = h_1(x^*) := g_3(g_2(g_1(x^*)))$ is increasing as well. Let us define the following function G

$$G(x) = h_1(x)\theta(g_2(g_1(x)))\frac{V_1 x}{K_1 + x} + h_1(x)\theta(g_2(g_1(x)))\frac{V_2 x}{K_2 + x} + \frac{1}{1 + k_c g_2(g_1(x))}\frac{V_3 x}{K_3 + x} + \alpha x. \tag{10}$$

It is clear that $G(0) = 0$ and $\lim_{x \rightarrow \infty} G(x) = \infty$. Now if $G(x^*) = \frac{V_4 C_{ex}}{K_4 + C_{ex}}$, then $x^* > 0$. We can obtain $h^* > 0, z^* > 0, m^* > 0$ by the above formulas and (m^*, z^*, h^*, x^*) is an equilibrium of (1-4). In addition, h^* satisfies $0 < h^* < 1$. Because of the boundness of the first three terms in (10), we can verify that there is a number $\bar{x} > 0$ such that $G(x)$ is monotone increasing for $x \geq \bar{x}$. By letting $\sigma = G^{-1}(\bar{x})$, we complete the proof. \square

We now consider the stability of the equilibrium of (1-4). The linearization of (1-4) at an equilibrium (m^*, z^*, h^*, x^*) is

$$\mathbf{X}' = \mathbf{A}\mathbf{X}, \tag{11}$$

where the variational matrix A is given by

$$A = \begin{pmatrix} -a_1 & 0 & 0 & a_2 \\ a_3 & -a_4 & 0 & 0 \\ 0 & a_5 & -a_6 & 0 \\ 0 & -a_7 & -a_8 & -a_9 \end{pmatrix}$$

and

$$a_1 = k_1(x^*)^3 + k_2 > 0, a_2 = 3k_1(c_1 - m^*)(x^*)^2, a_3 = k_3(c_2 - z^*), a_4 = k_3m^* + k_4 > 0,$$

$$a_5 = d_1\phi'(z^*)(1 - h^*) + d_2\phi'(z^*)h^* > 0,$$

$$a_6 = d_1\phi(z^*) + d_2(1 - \phi(z^*)) > 0,$$

$$a_7 = h^*\theta'(z^*)\frac{V_1x^*}{K_1 + x^*} + h^*\theta'(z^*)\frac{V_2x^*}{K_2 + x^*} - \frac{k_c}{(1 + k_cz^*)^2}\frac{V_3x^*}{K_3 + x^*}$$

$$a_8 = \theta(z^*)\frac{V_1x^*}{K_1 + x^*} + \theta(z^*)\frac{V_2x^*}{K_2 + x^*} > 0$$

and

$$a_9 = h^*\theta(z^*)\frac{V_1K_1}{(K_1 + x^*)^2} + h^*\theta(z^*)\frac{V_2K_2}{(K_2 + x^*)^2} + \frac{1}{1 + k_cz^*}\frac{V_3K_3}{(K_3 + x^*)^2} + \alpha > 0$$

If γ is an eigenvalue of A , then

$$\det \begin{pmatrix} -a_1 - \gamma & 0 & 0 & a_2 \\ a_3 & -a_4 - \gamma & 0 & 0 \\ 0 & a_5 & -a_6 - \gamma & 0 \\ 0 & -a_7 & -a_8 & -a_9 - \gamma \end{pmatrix} = 0,$$

which is

$$(-a_1 - \gamma)(-a_4 - \gamma)(-a_6 - \gamma)(-a_9 - \gamma) + a_2a_3(a_5a_8 + a_7a_6 + a_7\gamma) = 0.$$

Now we have the characteristic equation of A

$$\gamma^4 + B\gamma^3 + C\gamma^2 + D\gamma + E = 0. \quad (12)$$

where

$$B = a_1 + a_4 + a_6 + a_9, C = a_1a_4 + a_1a_6 + a_1a_9 + a_4a_9 + a_6a_9,$$

$$D = a_1a_4a_6 + a_1a_4a_9 + a_1a_6a_9 + a_4a_6a_9 + a_2a_3a_7,$$

and

$$E = a_1a_4a_6a_9 + a_2a_3a_7a_6 + a_2a_3a_5a_8.$$

The well known Routh-Hurwitz method is stated below without proof.

Lemma 3.7. [9] *The necessary and sufficient condition that the real parts of the roots of (12) shall all be negative is that B, C, D, E , and $BCD - D^2 - EB^2$ all be positive.*

Now we are in a position to give sufficient conditions to guarantee the stability of an equilibrium (m^*, z^*, h^*, x^*) .

Theorem 3.8. *If $B, C, D, E, BCD - D^2 - EB^2$ defined above are all positive, then the equilibrium (m^*, z^*, h^*, x^*) is locally asymptotically stable.*

If C_{ex} is greater than $1\mu M$, then (1–4) has only one equilibrium. For $C_{ex} = 1\mu M$, we calculate the unique equilibrium of (1–4) is $(x = 0.0073, m = 0.00004862, z = 0.0012, h = 0.0102657)$. The eigenvalues of A are

$$(-99.4948 + 4.2941 * i, -1.0077, -4.8013, -99.494 - 4.2941 * i)$$

and the equilibrium is locally stable. In fact, we can compute $B = 200.8899, C = 10399.13383, D = 50493.43576, E = 4978.097$ and $BCD - D^2 - EB^2 = 1.027343890 * 10^4$. The stability of the equilibrium is also confirmed by Theorem 3.8. We note that in this example, the real part of the complex eigenvectors is dominant, and the decaying oscillatory behavior associated with these roots is negligible.

4. Experimental and simulation results. A key feature of the model presented is the explicit separation of contributions to calcium sequestration. Mathematical analysis of mutants' response, where the key pumping proteins are absent, is easily carried out by simple deletion of relevant terms. Comparative analysis of the response of mutants to similar changes in external conditions is, of course, also feasible experimentally. In this section we present experimental determinations of these responses and compare them with results from simulations based on the model.

TABLE 1. Yeast strains.

Strain	Genotype
SEY6210 [13]	<i>Mata leu2-3,112 ura3-52 his3-Δ200 trp1Δ901 lys2-801 suc2-Δ9</i>
DB279 [10]	<i>Mata leu2-3,112 ura3-52 his3-Δ200 trp1Δ901 lys2-801 suc2-Δ9</i> <i>pmr1Δ::LEU2</i>
DB224 [10]	<i>Mata leu2-3,112 ura3-52 his3-Δ200 trp1Δ901 lys2-801 suc2-Δ9</i> <i>pmc1Δ::TRP1</i>
DB225 [10]	<i>Mata leu2-3,112 ura3-52 his3-Δ200 trp1Δ901 lys2-801 suc2-Δ9</i> <i>vcx1Δ::URA3</i>

4.1. Experimental procedure and results. The genotype of the strains used appears in Table 4.1. SEY6210 is the yeast strain without any mutations. DB224 is the yeast strain lacking the vacuolar calcium ATPase; this strain can be modeled by deletion of the second term in 4. DB279 lacks the endoplasmic reticulum calcium magnesium ATPase, and is modeled by deletion of the third term in 4. DB225 is the yeast strain lacking the vacuolar calcium exchanger, modeled by deletion of the fourth term in 4. Cells were transformed using the Yeast Easy Transformation Kit II (Zymo Research, Orange, CA) with the appropriate plasmid (SEY6210, DB224, and DB279 with pDB617 and DB225 with pEVP11/AEQ) and plated on selective media [5]. Yeast cultures were grown overnight in synthetic dextrose media with the appropriate supplements [5], back diluted into the same media in the morning, and grown to mid-log phase.

The plasmid carries a gene that codes for the apoaequorin protein [12]. This protein will luminesce (give off light) in response to calcium; the higher the calcium the more light it will give off. The apoaequorin must be reconstituted in order to luminesce. 10 μ l of 590 μ M coelenterazine (dissolved in methanol) was added to 0.2 ml of the cells, and the cells were incubated for 20 minutes at 30°C, in order to reconstitute the protein. Cells were then washed two times with media and resuspended in media. Cells were placed in a Sirius Luminometer (Berthold Detection Systems -USA, Oak Ridge, TN) and cytosolic calcium was measured as a

light pulse in response to a single pulse of 100 mM (final concentration) extracellular calcium. Examples of experimental results in these conditions are shown in Fig. 3. Similar experiments have been reported for wild strains, and mutants $vcx1\Delta$ and $pmc1\Delta$, with similar results [10, 11].

We note that the values of the parameters of the model have been selected to generate results similar to those presented in this section, but that a qualitative agreement has not been attempted. An specific difficulty in this task is the lack of a more precise determination of the relation between luminometer intensity units to cytosolic concentration. In the work of Miseta et al. [10] an approximate linear relation between the logarithms of luminosity and calcium concentration was obtained for the wild case, but further data for all other mutants is also necessary.

We note the following features of the experimental results. First, the data for wild type shows a sharp increase in cytosolic concentration of calcium upon introduction of a high concentration of ions to the extracellular environment. Cells are challenged with 100 mM extracellular calcium and internal calcium jumps precipitously. This calcium concentration then decays towards a new equilibrium value. The decay of the calcium concentration is monotonic. Next, the data for mutants with a deleted *PMC1* protein shows a very similar behavior with a lower maximum concentration. The mutant with deletion of *pmr1*, however, shows very similar behavior as that of the wild type, with only a slightly enhanced maximum concentration value. Finally, mutants with a deleted *VCX1* show two new distinct features. Their initial response is even larger than that of the wild and *pmr1* and *pmc1* deletion types and, in addition, its decay occurs much more slowly than the wild and other mutant types.

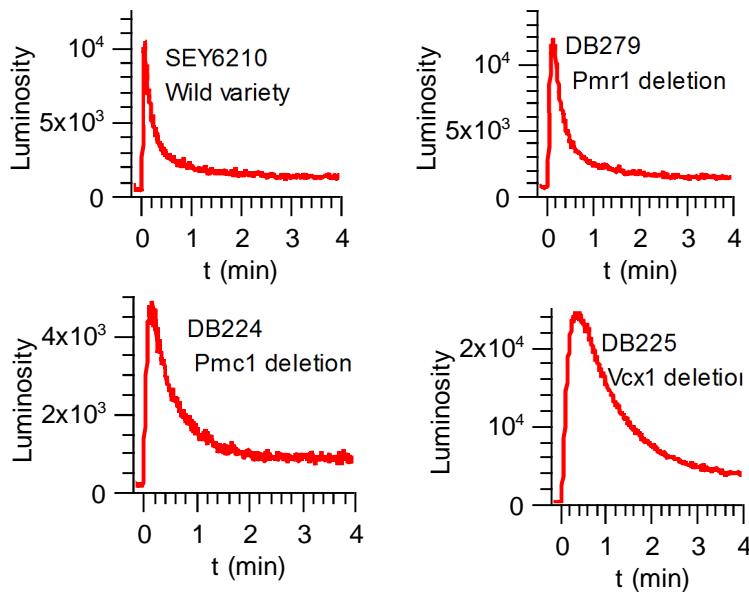


FIGURE 3. Experimentally observed luminosity versus time for four varieties of yeast cells. The luminosity indirectly reports the cytosolic calcium concentration.

4.2. Simulations and discussion. Next we show results of simulations of the model using the parameter set estimated by Cui and Kaandorp [3]. The simulation of mutants is obtained by simply setting to zero the terms related to activity of each of the deleted proteins. The deletions of *PMC1*, *PMR1* and *VCX1*, are obtained from elimination of the second, third, and fourth terms of the equation for x' in 4.

The numerical integration of the equations is carried out starting from an arbitrary state and allowing equilibration of the variables into a reference state with external calcium concentration of $0.01 \mu\text{M}$. The calcium is then elevated to 100 mM . Results of simulations in this case are shown in Fig. 4.

Simulations of the wild case behavior reproduce, broadly, the behavior observed in experiments. There is a sharp rise and second phase of slower decay towards an equilibrium state. The equilibrium concentration is much smaller than the maximum height of the peak. The parameters chosen by Cui and Kaandorp lead to a reasonable time scale for the decay of the initial concentration increase. The behavior in these simulations for deletions of *PMR1* and *VCX1*, for large external values of the external calcium is near identical to that of the wild case.

The most striking feature of these results, however, is the fact that the simulation of the deletion of *PMC1* results in a very different type of response. The response to a large external concentration of calcium converges to a state with very large values of cytosolic calcium and cannot be considered as a successful regulation. The *Pmc1p* term in the model is dominant with respect to other contributions and its absence allows equilibrium only through the extraction of Ca^{2+} ions by methods not directly associated with sequestration. The equilibrium in this case is established by the growth of the cell term. This behavior is observed in the *PMC1* deletion simulation for final external calcium concentrations C_{ex} values above (approximately) $100 \mu\text{M}$. For external concentrations below this threshold the response of the system is qualitatively similar to the wild and other mutant cases.

5. Conclusions and future studies. With the originally proposed selection of parameters for the model, we have found an important regime of external concentrations for which the model does not agree with observed behavior. Given these results, it would appear that a search for optimized parameters should be further attempted. However, several features of the system might be better addressed through modifications of the model. For example, as shown in Fig. 3, the near identical response of the wild and *PMC1* deletion indicates a quantitatively small role of *Pmc1p* in the regulatory network, while it is in fact the dominant term in the model. Another issue is the experimentally observed longer decay time for *VCX1* deletion. This points to the fact that *Pmr1p* and *Pmc1p* must be first produced in larger numbers by the cell to assist in regulation, and this process requires a relatively long time. Activated production of proteins might be best considered within models with time delays between activation events and protein production.

In spite of the problems above mentioned and the possible need for modified models, we note that the key results of the mathematical analysis presented remain schematically useful for a range of models. The activation functions studied have a broad scope of applications. The equilibrium analysis of other models without delay features might also run through very similar methods.

For both future experimental and theoretical investigations of the yeast cell system, it will be important to consider a larger variety of external influences. We

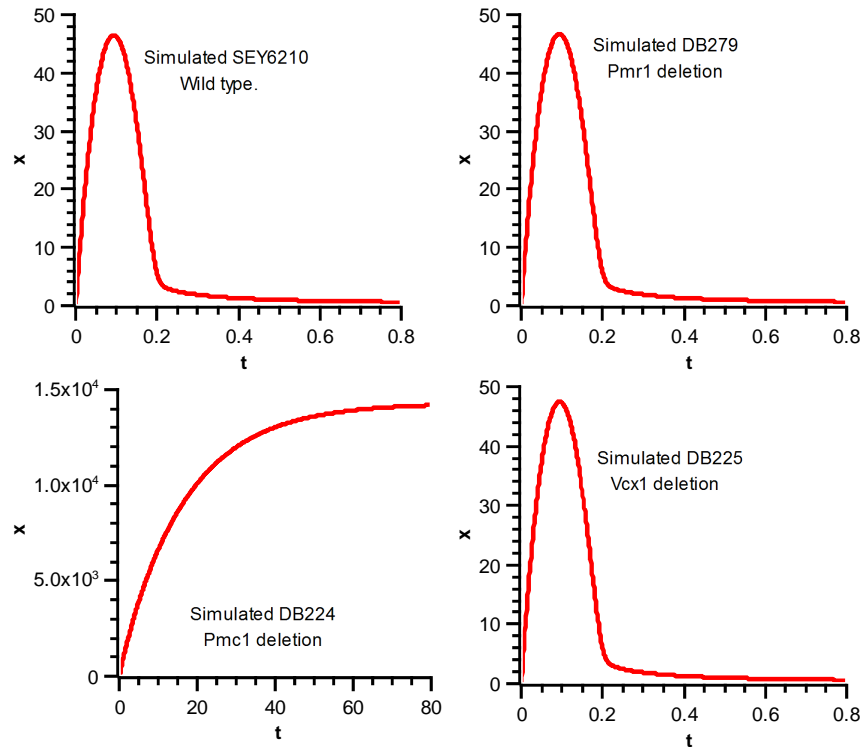


FIGURE 4. Simulation results for cytosolic calcium concentration.

propose in particular the use of sinusoidal and trains of step-like external calcium pulses. The use of such external variations have the ability of more directly revealing both stability properties and the presence of built-in delays in the calcium regulatory network. Current technology already allows the application of repeated accumulative pulses of external calcium. Our group of is currently working on analysis and experimental investigation of these cases.

Another important extension of this work will address the effects induced by the life cycle of the cells. Our experiments have probed the response of a yeast population to an increase in extracellular calcium. This response, however, is obtained from contributions of cells at different points in their life cycles. Specific features in the response of cells in one particular phase might be overshadow by the response of a larger population in a different phase. For example, RNA synthesis is extremely low in cells mitosis phase of the cell cycle; thus this population of cells (approximately 25% of the cells), would not be responding to the calcium with increased gene expression. The mathematical model does not address the individual nature of each of the cells, and in fact treat the population as if it were one whole. Future work will include synchronizing the cells so that we can assay the response to an extracellular calcium pulse in a population of cells that are not in the mitotic phase and thus are all able to respond with changes in gene expression.

Acknowledgements. Yeast strains were a kind gift of Bruce Horazdovsky, Mayo Clinic, Rochester, MN, and David Bedwell, University of Alabama at Birmingham. Yeast plasmids were kind gifts of Martha Cyert, Stanford University Medical Center (pEVP11/AEQ, [1]) and D. Bedwell (pDB617, [7]). The authors would like thank the reviewers for their suggestions, which helped to improve this paper.

Appendix A. Model parameters. The table below presents a description of the parameters of the model and its numerical values.

TABLE 2. Estimates of model parameters.

Parameter	Value	Description
K_1	$4.3 \mu\text{M}$	Binding constant of Pmc1p
K_2	$0.1 \mu\text{M}$	Binding constant of Pmr1p
K_3	$100 \mu\text{M}$	Binding constant of Vcx1p
K_4	$500 \mu\text{M}$	Binding constant of Cch1/Mid1 channel
V_1	$30000 \mu\text{M min}^{-1}$	Rate parameter of Pmc1p
V_2	$100 \mu\text{M min}^{-1}$	Rate parameter of Pmr1p
V_3	$10000 \mu\text{M min}^{-1}$	Rate parameter of Vcx1p
V_4	$1000 \mu\text{M min}^{-1}$	Rate parameter of Cch1/Mid1 channel
k_c	10	Feedback control constant
k_1	$500 (\mu\text{M})^{-3} \text{min}^{-1}$	Forward rate constant of m -equation in (1)
k_2	100min^{-1}	Backward rate constant of m -equation in (1)
k_3	$5 (\mu\text{M})^{-3} \text{min}^{-1}$	Forward rate constant of z -equation in (2)
k_4	5min^{-1}	Backward rate constant of z -equation in (2)
c_1	$25 \mu\text{M}$	Total calmodulin concentration
c_2	$25 \mu\text{M}$	Total calcineurin concentration
d_1	0.4min^{-1}	Nuclear import rate constant
d_2	0.1min^{-1}	Nuclear export rate constant
N	13	Number of regulatory phosphorylation sites
λ	5	Increment factor
α	0.006	Growth rate constant

Appendix B. Proof of Lemmas. In this appendix, we provide proof of Lemmas 3.1 and 3.2.

B.1. Proof of Lemma 3.1. Proof. Let

$$\zeta(x) = \frac{x^{N+1} - 1}{x - 1} = \sum_{i=0}^N x^i > 0, x \in [0, \infty).$$

It is easy to see that $\zeta(x)$ and $\phi(x) = \frac{1}{1+10^{-\frac{N}{2}} \frac{\zeta(\frac{\lambda}{x})}{\zeta(\frac{1}{x})}}$ are continuously differentiable on $(0, \infty)$. We can verify that $\lim_{x \rightarrow 0} \zeta(x) = 1$, $\lim_{x \rightarrow 0} \zeta'(x) = 1$, $\lim_{x \rightarrow \infty} \zeta(x) = \infty$, $\lim_{x \rightarrow \infty} \zeta'(x) = \infty$, $\lim_{x \rightarrow 0} \frac{\zeta(\lambda x)}{\zeta(x)} = 1$, and $\lim_{x \rightarrow \infty} \frac{\zeta(\lambda x)}{\zeta(x)} = \lambda^N$. Therefore, $\lim_{x \rightarrow 0} \phi(x) = \frac{1}{1+10^{-\frac{N}{2}} \lambda^N} < 1$ and $\lim_{x \rightarrow \infty} \phi(x) = \frac{1}{1+10^{-\frac{N}{2}}} < 1$. Thus, $\phi(x)$ is continuous on $[0, \infty)$.

In order to find the derivative of $\phi(x)$, We first calculate the derivative of $\frac{\zeta(\lambda x)}{\zeta(x)}$. Since $\zeta'(x) = \sum_{i=1}^N ix^{i-1}$, the derivative of $\frac{\zeta(\lambda x)}{\zeta(x)}$ can be calculated as

$$\frac{(\zeta(\lambda x))'\zeta(x) - \zeta(\lambda x)\zeta'(x)}{(\zeta(x))^2} = \frac{\sum_{k=0}^N \sum_{i=1}^N i\lambda^i x^k x^{i-1} - \sum_{k=1}^N \sum_{i=0}^N kx^{k-1} \lambda^i x^i}{(\zeta(x))^2}.$$

By regrouping the terms with $k = 0, i = 0$, the above term becomes

$$\frac{\sum_{i=1}^N i\lambda^i x^{i-1} - \sum_{k=1}^N kx^{k-1} + \sum_{k=1}^N \sum_{i=1}^N i\lambda^i x^k x^{i-1} - \sum_{k=1}^N \sum_{i=1}^N kx^{k-1} \lambda^i x^i}{(\zeta(x))^2},$$

which is

$$\frac{\sum_{i=1}^N i(\lambda^i - 1)x^{i-1} + \sum_{k,i=1}^N (i - k)\lambda^i x^{i+k-1}}{(\zeta(x))^2}.$$

It is easy to see that $\sum_{i=1}^N i(\lambda^i - 1)x^{i-1} > 0$ because of $\lambda > 1$ and $\sum_{k,i=1}^N (i - k)\lambda^i x^{i+k-1} > 0$ because of the symmetry of i, k . Thus the derivative of $\frac{\zeta(\lambda x)}{\zeta(x)}$ is positive and continuous for $x \in [0, \infty)$. We now turn to $\phi'(x)$. By the quotient rule, we have

$$\phi'(x) = \frac{10^{-\frac{N}{2}} \left(\frac{\zeta(\lambda x)}{\zeta(x)}\right)' \Big|_{\frac{1}{x}} \frac{1}{x^2}}{\left(1 + 10^{-\frac{N}{2}} \frac{\zeta(\frac{\lambda}{x})}{\zeta(\frac{1}{x})}\right)^2} = \frac{10^{-\frac{N}{2}} \frac{\sum_{i=1}^N i(\lambda^i - 1)(\frac{1}{x})^{i-1} + \sum_{k,i=1}^N (i - k)\lambda^i (\frac{1}{x})^{i+k-1}}{(\zeta(\frac{1}{x}))^2} \frac{1}{x^2}}{\left(1 + 10^{-\frac{N}{2}} \frac{\zeta(\frac{\lambda}{x})}{\zeta(\frac{1}{x})}\right)^2},$$

Recall that $\zeta(x) = \frac{x^{N+1}-1}{x-1} = \sum_{i=0}^N x^i$, we further have

$$\phi'(x) = \frac{10^{-\frac{N}{2}} \frac{\sum_{i=1}^N i(\lambda^i - 1)(\frac{1}{x})^{i-1} + \sum_{k,i=1}^N (i - k)\lambda^i (\frac{1}{x})^{i+k-1}}{(\sum_{i=0}^N (\frac{1}{x})^{i-1})^2} \frac{1}{x^2}}{\left(1 + 10^{-\frac{N}{2}} \frac{\zeta(\frac{\lambda}{x})}{\zeta(\frac{1}{x})}\right)^2},$$

Thus, $\phi'(x) > 0, x \in (0, \infty)$, $\lim_{x \rightarrow 0} \phi'(x) = 0$ and $\lim_{x \rightarrow \infty} \phi'(x) = 0$. □

B.2. Proof of Lemma 3.2. *Proof.* Again let

$$\zeta(x) = \frac{x^{N+1} - 1}{x - 1} = \sum_{i=0}^N x^i > 0, x \in (0, \infty).$$

Then

$$\theta(x) = \frac{1 + 10^{-\frac{N}{2}}}{\zeta(\frac{1}{x}) + 10^{-\frac{N}{2}} \zeta(\frac{\lambda}{x})},$$

$$\lim_{x \rightarrow 0} \theta(x) = 0,$$

and

$$\lim_{x \rightarrow \infty} \theta(x) = 1.$$

One can verify that

$$\theta'(x) = \frac{(1 + 10^{-\frac{N}{2}}) \left(\zeta'(\frac{1}{x}) \frac{1}{x^2} + 10^{-\frac{N}{2}} \lambda \zeta'(\frac{\lambda}{x}) \frac{1}{x^2}\right)}{\left(\zeta(\frac{1}{x}) + 10^{-\frac{N}{2}} \zeta(\frac{\lambda}{x})\right)^2}$$

Since $\zeta' > 0$, we have $\theta'(x) > 0$ for $x \in (0, \infty)$. We can further calculate the limits of θ at zero and infinity.

$$\lim_{x \rightarrow 0} \theta'(x) = 0, \lim_{x \rightarrow \infty} \theta'(x) = 0.$$

This completes the proof. \square

REFERENCES

- [1] A. F. Batiza, T. Schulz and P. H. Masson, *Yeast respond to a hypotonic shock with a calcium pulse*, J. Biol. Chem., **38** (1996), 23357–23362.
- [2] K. M. Cunningham and G. R. Fink, *Calcineurin inhibits VCX1-dependent H⁺/Ca²⁺ exchange and induces Ca²⁺ ATPases*, in “Saccharomyces Cerevisiae,” Mol Cell Biol., **16**(5) (1996), 2226–37.
- [3] J. Cui and J. Kaandorp, *Mathematical modeling of calcium homeostasis in yeast cells*, Cell Calcium, **39** (2006), 337–348.
- [4] E. G. Locke, M. Bonilla, L. Liang, Y. Takita and K. W. Cunningham, *A homolog of voltage-gated Ca²⁺ channels stimulated by depletion of secretory Ca²⁺ in yeast*, Mol. Cell. Biol., **20** (2000), 6686–6694.
- [5] C. Guthrie and G. R. Fink, “Guide to Yeast Genetics and Molecular Biology,” in Methods in Enzymology, Academic Press San Diego CA, **194** (1991).
- [6] W. M. Hirsch, H. Hanisch and J. P. Gabriel, *Differential equation models of some parasitic infections: Methods for the study of asymptotic behavior*, Comm. Pure Appl. Math., **38** (1985), 733–753.
- [7] R. Kellermayer, D. P. Aiello, A. Miseta and D. B. Bedwell, *Extracellular Ca²⁺ sensing contributes to excess Ca²⁺ accumulation and vacuolar fragmentation in a pmr1 mutant of S. cerevisiae*, J. Cell Sci., **8** (2003), 1637–1646.
- [8] D. P. Matheos, et al., *Tcn1p/Crz1p, A calcineurin-dependent transcription factor that differentially regulates gene expression in Saccharomyces cerevisiae*, Genes Dev., **11**(24) (1997), 3445–58.
- [9] J. D. Murray, “Mathematical Biology,” Springer, 1989.
- [10] A. Miseta, L. Fu, R. Kellermayer, J. Buckley and D.M. Bedwell, *The Golgi apparatus plays a significant role in the maintenance of Ca²⁺ homeostasis in the vps33 vacuolar biogenesis mutant of Saccharomyces cerevisiae*, J. Biol. Chem., **9** (1999), 5939–5947.
- [11] A. R. Kellermayer, D. P. Aiello, L. Fu and D. M. Bedwell, *The vacuolar Ca²⁺/H⁺ exchanger Vcx1p/Hum1p tightly controls cytosolic Ca²⁺ levels in S. cerevisiae*, FEBS Lett., **451** (1999), 132–6.
- [12] J. Nakajima-Shimada, H. Iida, F. I. Tsuji and Y. Anraku, *Monitoring of intracellular calcium in Saccharomyces cerevisiae with a apoaequorin cDNA expression system* Proc. Natl. Acad. Sci., **15** (1991), 6878–6882.
- [13] J. S. Robinson, D. J. Klionsky, L. M. Banta and S. D. Emr, *Protein sorting in Saccharomyces cerevisiae: Isolation of mutants defective in the delivery and processing of multiple vacuolar hydrolases*, Mol. Cell Biol., **11** (1988), 4936–4948.
- [14] C. Salazar and T. Hofer, *Allosteric regulation of the transcription factor NFAT1 by multiple phosphorylation sites: A mathematical analysis*, J. Mol. Biol., **327** (2003), 31–45.
- [15] A. M. Stathopoulos and M. S. Cyert, *Calcineurin acts through the CRZ1/TCN1-encoded transcription factor to regulate gene expression in yeast*, Genes Dev., **11**(24) (1997), 3432–44.
- [16] Jinfeng Teng, Rika Goto, Kazukolida, Itaru Kojima and Hidetoshi Iida, *Ion-channel blocker sensitivity of voltage-gated calcium-channel homologue Cch1 in Saccharomyces cerevisiae*, Microbiology, **154** (2008), 3775–3781.
- [17] Y. Q. Zhang and R. Rao, *A spoke in the wheel: Calcium spikes disrupt yeast cell cycle*, Cell Cycle, **7**(7) (2008), 870–3.

Received October 2008; revised May 2009.

E-mail address: francisco.solis@asu.edu

E-mail address: Eden.Tanzosh@asu.edu

E-mail address: pamela.marshall@asu.edu

E-mail address: wangh@asu.edu